11th World Congress on Computational Mechanics (WCCM XI)
5th European Conference on Computational Mechanics (ECCM V)
6th European Conference on Computational Fluid Dynamics (ECFD VI)
E. Oñate, J. Oliver and A. Huerta (Eds)

MODELING OF MICROSTRUCTURE DEVELOPMENT DURING HOT DEFORMATION AND SUBSEQUENT ANNEALING OF PRECIPITATES CONTAINING AA6016

FENG JIAO*, VOLKER MOHLES†, ALEXIS MIROUX† AND CHRISTIAN BOLLMANN†

* Institute of Physical Metallurgy and Metal Physics, RWTH Aachen University
Kopernikusstr. 14, Aachen, D-52074, Germany. e-mail: jiao@imm.rwth-aachen.de

†Institute of Physical Metallurgy and Metal Physics, RWTH Aachen University
Kopernikusstr. 14, Aachen, D-52074, Germany. e-mail: mohles@imm.rwth-aachen.de

†Materials innovation institute (M2i), TU-Delft
Mekelweg 2, 2628 CD Delft, The Netherlands. e-mail: a.g.miroux@tudelft.nl

†Aleris Rolled Products Germany GmbH
Vaalser Str. 460, Aachen, D-52074, Germany. e-mail: christian.bollmann@aleris.com

Key words: Commercial Al-Mg-Si alloy, hot deformed microstructure, recrystallization driving force, Zener drag force, partial recrystallization, modeling of recrystallization

Abstract. Microstructure and microchemistry evolution during hot deformation and subsequent annealing of a commercial Al-Mg-Si alloy were experimentally investigated using electron backscatter diffraction (EBSD) and SEM. Meanwhile, a through-process model framework consisting of the deformation model GIA-3IVM+ and the recrystallization (RX) model CORe was utilized to simulate the microstructure evolution during the processing. Based on the experimental observations a new model for the RX driving force in particular after hot deformation and its evolution during subsequent annealing is proposed. Unlike a driving force model for cold deformed materials proposed recently, the geometrically necessary dislocations (GNDs) are taken into account in the new model for hot deformed materials, in which the deformation stored energy is normally very low. Furthermore, the static recovery of statistical stored dislocations, which decreases the RX driving force, is terminated in the new model at a certain level. This is based on the fact that after evolving into subgrain boundaries, dislocation cell walls will no longer change (apart from very slow subgrain growth). Fine precipitates exhibit back-driving forces on the moving grain boundary, namely the Zener drag force. This diminishes the effective driving force for RX in the deformed grains. Implementing these aspects into the RX model CORe, the partial RX in materials deformed at two variant conditions

could be modeled. The predicted microstructural results are consistent with the experimental observation in terms of RX kinetics, recrystallized grain structure and size, and recrystallized volume fraction.

1 INTRODUCTION

In the process chain of aluminum sheet production, microstructure evolution during the early stages of processing such as break-down hot rolling and tandem hot rolling are of high importance. These early steps define the initial state of the material for subsequent processing and hence have a strong impact on the development of microstructure and the final sheet properties. Nevertheless, the complex nature of microstructural transformation during hot rolling is difficult to investigate, since a series of metallurgical phenomena such as work hardening, precipitation, recovery and RX are involved and may interact with each other. Unfortunately, it is practically impossible to obtain and characterize samples of the intermediate material state from the multi-pass hot rolling line. In light of the obstacles to experimental investigations of sheet production, and hot rolling in particular, numerical simulations using physics based models offer a great complement to study causes and effects of processing details. In recent years, through-process modeling of microstructure and texture evolution has been established for this. At the Institute of Physical Metallurgy and Metal Physics (IMM) of the RWTH Aachen University, an integrated model framework consisting of a group of sub-models has been developed, each of them handling specific aspects of the microstructural transformation. In the current study, several models including the deformation model GIA-3IVM+ and the RX model CORe are chosen to model the microstructure and texture development of AA6016 during hot plane strain compression (PSC) and the subsequent annealing. The experimental conditions are chosen to be very close to those in the first steps of break-down hot rolling. However unlike in industrial rolling, experimental characterization of the material state is possible. The computer models are adjusted and calibrated to simulate the experimental observations. In perspective, this will enable to simulate microstructure and property evolution throughout sequences of hot rolling passes in dependence of the initial material state after homogenization.

2 MODELS

2.1 The deformation model GIA-3IVM+

Deformation texture model (GIA). The texture development during hot deformation was modeled using the grain interaction (GIA) model [1, 2]. The GIA model is an improved FC-Taylor model which considers interactions between neighboring grains by describing the behavior of an eight-grain aggregate (2×2×2) embedded in a homogeneous surrounding. The deformation of the complete aggregate is fully prescribed by the macroscopic strain tensor, which can follow any strain path as needed for rolling. In the present

setup, only PSC is considered in full equivalence to the present experimental conditions. Between the eight grains of an aggregate, relaxation of the prescribed strain is allowed leading to individual deformation of each single grain. The resulting strain incompatibilities are compensated by the introduction of geometrically necessary dislocations (GNDs) at the grain boundaries and the interfaces to the surrounding. The active slip systems of all grains are determined by minimizing the dissipation energy from dislocation slip in all active slip systems. In this minimization, an additional energy penalty is considered for the newly generated GNDs, leading to grain interaction. The individual choice of active slip systems leads to individual lattice rotations of the grains. For one GIA simulation, 500 aggregates with 4000 grain orientations reflecting the initial texture are deformed as prescribed. The distribution of lattice rotations describes the texture evolution, while the individual deformations of all grains describe the evolution of a strain distribution. The latter, in combination with the work-hardening and recovery model 3IVM+ (see below), provides a distribution of dislocation densities and hence driving forces for RX.

Work-hardening and recovery model (3IVM+). The three internal variables model (3IVM) is a statistical dislocation density based work-hardening and recovery model [3, 4, 5, 6, 7]. Within each grain of the GIA model individually, it serves to calculate the flow stress during deformation in dependence of temperature and strain rate, which may both vary with time. The model assumes the development of a cellular dislocation substructure during deformation, and is based on the densities of three populations of dislocations as the microstructural state variables: the immobile dislocations in the cell interior (ρ_i) and in the cell walls (ρ_w), as well as the mobile dislocations (ρ_m), which accommodate the plastic deformation. The evolution of these dislocation densities is described by their generation and annihilation rates. For instance, mobile dislocations are generated with increasing strain and later turned into immobile ones by statistical descriptions of dipole and lock formation. For recovery, the dislocation annihilation rates considered include a mechanical, strain dependent term as well as terms for thermally activated climb and cross slip. The latter recovery terms are also used to simulate static recovery occurring concurrent with recrystallization within the model CORe (see below). The model parameters, which all have a physical meaning and are bound to reasonable value ranges, were calibrated by calculating flow curves and fitting them to those measured by PSC in the relevant temperature and strain rate ranges. The fitted parameters used for all subsequent simulations are listed in table 1.

Coupling of GIA and 3IVM+. For the GIA simulations the critical shear stress is provided by 3IVM+ for each grain individually. For this, the GIA model provides the temperature, the instantaneous strain rate and the number of active slip planes in the same manner as previously described for the predecessor 3IVM [8]. The number of slip planes influences the probabilities of certain dislocation interactions [3, 4, 5] and hence has an impact on the evolution of the different dislocation densities ($\rho_\mathrm{i,w,m}$). The coupling of GIA and 3IVM+ realizes the prediction of orientation and dislocation densities of each single grain.

Table 1: Parameter set of 3IVM+ obtained from flow curve fitting.

Parameter	Value	Description
d_{annihil}	1.73 b	Critical distance for dislocation annihilation
d_{lock}	1.43 b	Critical distance for dislocation climbing
d_{immob}	2.26 b	Critical distance for immobilization
d_{clear}	3.57 b	Critical distance for clearing effect
d_{climb}	7.61 b	Critical distance for dislocation climbing
f_{w}	0.19	Volume fraction of dislocation cell walls
β_{i}	110.59	Constant for the spacing of internal dislocations
β_{w}	53.63	Constant for the spacing of wall dislocations
α_{Taylor}	0.61	Factor of Taylor passing stress
V_{cross}	91.29 b^3	Activation volume for cross slip
Q_{cross}	1.55 eV	Activation energy for cross slip
Q_{climb}	1.21 eV	Activation energy for climbing
$\rho_{\text{m,0}}$	5.8×10^9 m^{-2}	Initial mobile dislocation density
$\rho_{\text{i,0}}$	6.4×10^9 m^{-2}	Initial internal dislocation density
$\rho_{\text{w,0}}$	4.3×10^{12} m^{-2}	Initial cell wall dislocation density
$\sigma_{\text{therm,solute}}$	30.0 MPa	Thermally activated hardening effect of solutes extrapolated to T = 0 K, $c_{\text{solute}} = 100\%$
$\sigma_{\text{atherm,solute}}$	85.2 MPa	Athermal hardening effect of solutes extrapolated to $c_{\text{solute}} = 100\%$
σ_{particle}	1000 MPa	Shear stress inside a particle
N	3	Number of active slip planes

2.2 The RX model CORe

During annealing RX takes place, strongly influenced by the dislocation density, fine particles, solute atoms, and also by changes in their respective quantities. The microstructural evolution during annealing was modeled by the CORe model, which is mainly a celluar automaton for RX growth coupled with a nucleation model. CORe is interfaced to sub-models to consider other influencing phenomena, like changes in the microchemical state. The initial material state and geometry for CORe is essentially provided by GIA-3IVM+. The geometry is a block of equally sized cuboid grains, each of which has the lattice orientation, dislocation density and shape of one GIA grain. The grains are subdivided into cells which can change their state from deformed to recrystallized continuously in order to simulate RX growth. Initially, each RX nucleus is represented by one cell.

RX nucleation. RX nucleation has its origin in the deformed microstructure. For simulating it, calculated quantities from the deformation models are used to describe

the probability of different nucleation mechanisms to become active. These mechanisms include grain boundary and shear band nucleation from the GIA model [2, 8], transition band nucleation from the GIA-Split-Up model [2] as well as particle stimulated nucleation (PSN) from GIA-DZ [9]. The absolute nuclei numbers play an essential role for the RX texture and grain size. They are calculated from the mechanical instability of a bulging grain boundary as described in [10, 11]. For this calculation the subgrain size is needed, which in turn is calculated from the dislocation density [11].

In the present study focusing on RX kinetics but not texture, grain boundary nucleation was selected as the only mechanism. The omission of PSN and shear band nucleation is justified due to the high deformation temperature [12, 13]. Transition band nucleation was suppressed in this preliminary modeling in order to simplify the model calibration to describe the final grain size, the kinetics, and the final recrystallized volume fraction in particular. The distinction between different nuclei may be considered later in a refined investigation. Nucleation was assumed to be site-saturated, i.e. all nuclei were initiated and ready to grow from the beginning of annealing.

RX growth. Once a viable nucleus is formed, it can grow into the surroundings. The grain boundary migration rate v of the nucleus can be expressed as

$$v = m \cdot p_{\text{eff}} \tag{1}$$

where m is the boundary mobility and p_{eff} is the effective driving force, which equals the driving force (p_{driv}) reduced by the back-driving Zener force (p_{Z}). The boundary mobility is considered as a function of the misorientation between the adjacent grains. In the model the boundary mobility is described by three classes: a low mobility for low angle grain boundaries, a high mobility for high angle grain boundaries, and a particularly high mobility for boundaries close to a 40° <111> misorientation. In respect of their temperature dependencies, all these mobility classes are described by an Arrhenius term to reflect their thermal activation. Furthermore, solute drag is considered in the CORe model as described in [11, 14]. The driving force for RX is given by the deformation stored energy in each grain individually as described by

$$p_{\text{driv}} = \frac{1}{2} \cdot G \cdot b^2 \cdot \rho_{\text{total}} \tag{2}$$

where G is the shear modulus, and b is the Burgers vector. In the original formulation [14], the dislocation density ρ_{total} is comprised of the immobile dislocations in the cell interior (ρ_{i}) and in the cell walls (ρ_{w}), which are obtained from the previous GIA-3IVM+ deformation simulation for each grain. In the present investigation, the GNDs (ρ_{GND}) were accounted additionally for the driving force. The total dislocation density is expressed as stored energy in each grain individually as described by

$$\rho_{\text{total}} = (1 - f_{\text{w}}) \cdot \rho_{\text{i}} + f_{\text{w}} \cdot \rho_{\text{w}} + f_{\text{GND}} \cdot \rho_{\text{GND}} \tag{3}$$

where f_{w} is the volume fraction of the dislocation cell walls, which is part of the 3IVM+ fitting parameters (table 1). ρ_{GND} is calculated from the strain relaxations by the texture

model GIA. Thus the obtained ρ_{GND} is highly dependent on the total strain and the activation of the slip systems in each grain, however, it is independent of the flow stress. This feature is important for hot deformation modeling, especially in the steady state regime (constant flow stress), in which the state variables ρ_{i} and ρ_{w} remain constant. The factor f_{GND} is introduced here and chosen equal to 0.05. The reason for this factor is that in the model GIA, the introduction of GNDs is meant to be an energetic penalty for the grain relaxation, which requires GNDs, during energy minimization of the aggregates. However it is known from calorimetric experiments that in order to create a certain amount of dislocation density, a much higher amount of energy (factor 10-20) is needed than just the energy of the GNDs themselves. Hence GND is probably overestimated in the GIA model by this factor.

In the presence of fine particles, the moving boundary can be hindered significantly by the Zener drag force. The effective driving force is decreased correspondingly. In cases where the Zener drag force is equal to or larger than the driving force p_{driv}, the effective driving force p_{eff} vanishes, hence the boundary will be pinned. The overall drag force p_{Z} is calculated as

$$p_{\mathrm{Z}} = -\frac{3}{2} \cdot \gamma \cdot \frac{f_{\mathrm{p}}}{r_{\mathrm{p}}} \tag{4}$$

where γ denotes the grain boundary energy, and f_{p} and r_{p} represent the volume fraction and the average radius of the fine particles, respectively.

Recovery. The recovery part of 3IVM+ had been integrated into the CORe model on a grain scale, so that recovery and hence the driving force evolution during annealing is simulated for each grain individually [14]. 3IVM+ considers two thermally activated recovery mechanisms, namely the annihilation of cell wall and cell interior dislocations by climb and by cross slip [6, 7]. The total annihilation rate of the dislocations is assumed to be the sum of the independent rates by both mechanisms. Nevertheless, the GNDs are treated as non-recoverable as mentioned previously.

In the current simulation procedure, static recovery during annealing is terminated when a certain criterion is met, instead of being operative until complete annihilation of ρ_{i} and ρ_{w} as in the original setup [14]. This is mainly based on the fact that after evolving into subgrain boundaries, dislocation cell walls will no longer change significantly. During recovery simulation, ρ_{i} and ρ_{w} decrease continuously, and so does the difference between them. The relative difference between the two dislocation densities was used to define the criterion for recovery termination:

$$\frac{\rho_{\mathrm{w}} - \rho_{\mathrm{i}}}{\rho_{\mathrm{i}}} \leq \eta \tag{5}$$

where η is a parameter. By selecting the value of η, the level of recovery will be fixed. Since each grain has specific recovery kinetics, the time for reaching the criterion differs from grain to grain. The same criterion, referred to as convergence approach, had originally been introduced to define an incubation time for RX nucleation [14].

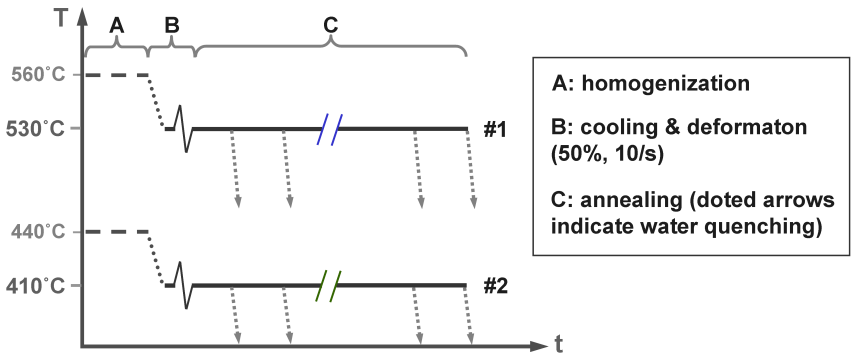

Figure 1: Thermomechanical history of AA6016 samples along two processing routes.

3 EXPERIMENTAL PROCEDURE

The experimental procedure is schematically represented in figure 1. The initial state of the material is as-homogenized. Two different homogenization thermal cycles were applied, which resulted in different microchemical states. Nevertheless, according to the experimental characterization the states of α-dispersoids in both cases are similar: the mean radius is about 51 nm and the volume fraction is 0.086%. Starting from the two homogenized states the materials were processed similarly further along the process routes 1 and 2, which are referred to subsequently by blue (1) and green (2) colors. In figure 1 the end stages of the homogenization thermal cycles are represented by dashed lines with the finishing temperatures of 560°C and 440°C for the routes 1 and 2, respectively. After homogenization the material was slightly cooled with a temperature drop of 30°C, and then subjected to PSC with a thickness reduction of 50% at a strain rate of 10/s. After deformation the material was annealed isothermally at this same temperature. After differing annealing times, equivalent samples of initially the same material were quenched in water to preserve their respective microstructures. Later on the characterization of these microstructures was performed using EBSD.

4 RESULTS

4.1 Hot deformed microstructure

The hot deformed microstructures are measured by EBSD and represented as band quality maps. In the case of route 1 (530°C), the deformed microstructure consists of a well defined subgrain structure because of strong dynamic recovery (figure 2.a). In contrast, after lower temperature deformation (route 2, 410°C) the substructure contains large amounts of crystal defects, mainly dislocation structures, as indicated by the band quality map (figure 2.c). Altogether the deformation at lower temperature lead to a finer substructure than the one deformed at higher temperature, indicating higher deformation stored energy in the former case. Another characteristic aspect of the substructures in

both cases is that deformation is inhomogeneous: some deformed grains in figures 2.a and 2.c have formed a fine subgrain structure, whereas others consist of subgains that are much larger in comparison.

Hot deformation was modeled for both routes by simulating 4000 grains with GIA-3IVM+. The simulated total dislocation density ρ_{total} (equation 3) is plotted for all grains as a relative frequency distribution in figures 2.b and 2.d. The model predicts the right tendency in the deformation stored energy for the different deformation conditions: the calculated mean dislocation density of deformation at 410°C is almost three times as high as the one for deformation performed at 530°C. Besides, the inhomogeneity of deformation observed experimentally is reflected in the simulation results as well: both distributions in figures 2.b and 2.d are rather wide, and they seem to indicate two peaks (figure 2.d in particular), just like the subgrain sizes visible in the corresponding micrographs 2.a and 2.c.

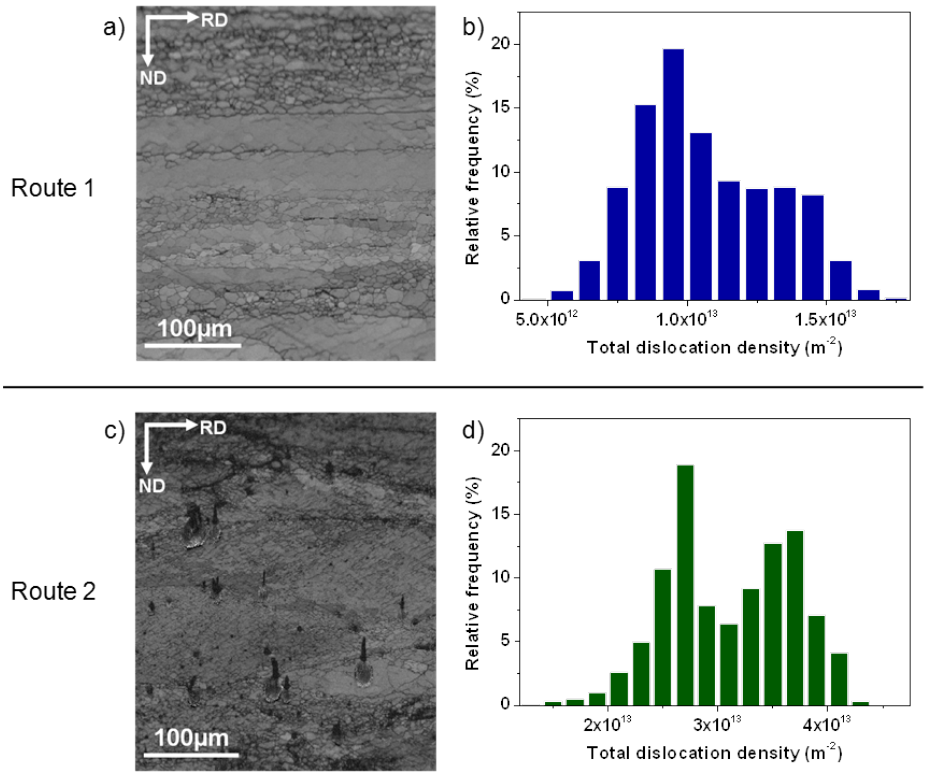

Figure 2: Hot deformed microstructure (a,c) represented as band quality maps measured by EBSD, and (b,d) simulated distribution of dislocation density after hot deformation. (a,b) Route 1, 530°C; (c,d) route 2, 410°C.

It should be noted that the double peak nature of the driving force seems to be a rather stable simulation result. This has been found by further GIA-3IVM+ simulations with the same processing conditions, but using a 3IVM+ parameter set that differs slightly

from the one given in table 1, but provides essentially the same quality of flow curve prediction.

4.2 RX behavior

The microstructure of the material after various annealing times was characterized by means of EBSD. From the respective micrographs the corresponding recrystallized volume fraction was obtained. The resulting RX kinetics is presented in figures 3.a and 3.b for routes 1 and 2 respectively. It is obvious that RX ceased after reaching saturation in both routes. The maximum recrystallized fraction is around 50% and 40% for the processing temperatures of 530°C and 410°C, respectively. The recrystallized grains of route 1 are coarser than those processed at lower temperature in route 2.

The annealing process was simulated by the CORe model. Its input microstructure was the deformed microstructure provided by GIA-3IVM+. Static recovery was terminated by the approach expressed in equation 5, with the parameter η=0.8 for both cases. This choice results in a rather short operating time of recovery.

For the route 1, the Zener drag force is calculated according to equation 4 using the experimental observed state of the α-dispersoids. Whereas, the Zener drag force was adaptively increased by a factor of 4 for the route 2, since another population of fine particles were formed during processing at 410°C (figure 4.a) that had not been present after homogenization at 440°C. In comparison, materials processed at 530°C are without the new precipitates (figure 4.b). These fine particles always protruded from the sample surface after electro-polishing. Therefore they are clearly visible using the secondary electrons under SEM, however, the α-dispersoids are almost invisible (figure 4.a, 4.b).

The simulated RX behavior is represented in figure 3 in terms of the kinetics and the recrystallized grain size. Generally, the simulation agrees very well with the experimental result in light of the experimental errors. For both routes, the partial RX was successfully modeled by the setup described. Considering the size distribution of the recrystallized grains, the modeled most frequent grain size is a bit larger than the experimentally observed one in both cases. But more importantly, the predicted number density of the very large recrystallized grains is consistent with experiments.

5 DISCUSSION

The hot deformed microstructure was studied experimentally and numerically. The inhomogeneous deformation behavior on the grain to grain scale was successfully modeled in a qualitative manner. For both deformation temperatures a wide spectrum of dislocation density exists among the 4000 grains simulated. However, EBSD is not sufficient to characterize all respects of the deformed microstructure. For a better understanding of the dynamically recovered microstructure, further investigations using transmission electron microscopy are prepared at present to characterize the structure of dislocation cells and / or subgrains. This will give clearer guidance on how to model the static recovery during

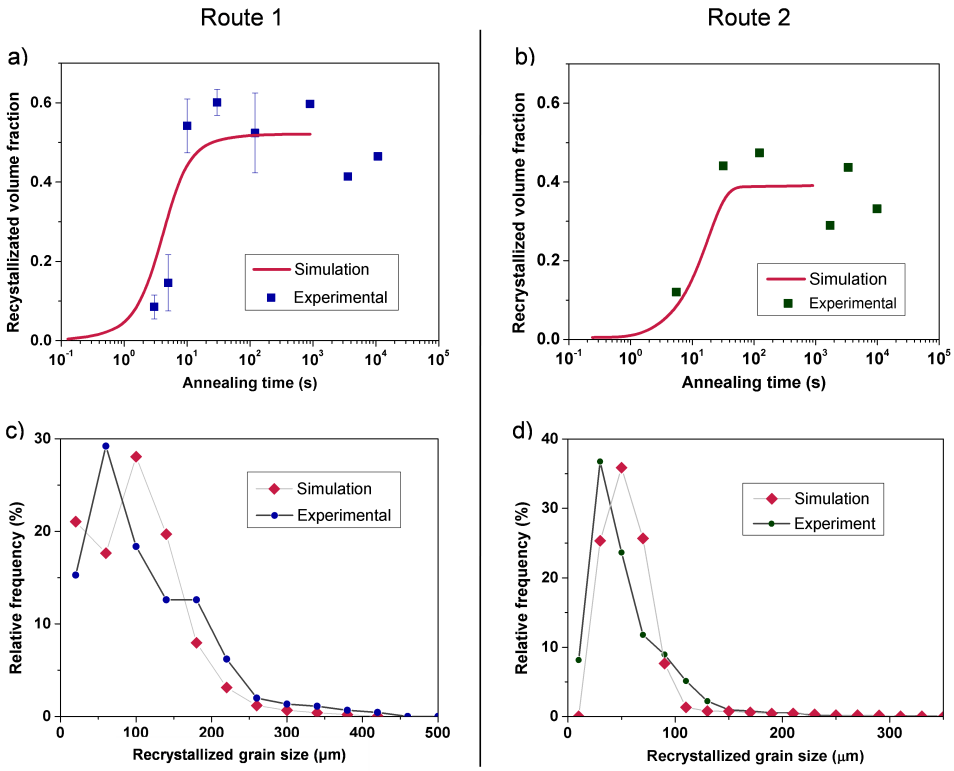

Figure 3: Experimental and simulated recrystallization kinetics (a,b) and the size distribution of the recrystallized grains: (a,c) route 1, 530°C; (b,d) route 2, 410°C.

subsequent annealing.

The partial RX can be interpreted as the consequence of only a part of the deformed grains having an effective driving force due to the presence of a Zener drag force. Since the same drag force p_Z was applied to all the deformed grains in the simulations, it is the inhomogeneous dislocation density on the grain to grain scale that leads to only partial RX.

For modeling the RX, a new driving force model accounting several assumptions was applied. These assumptions were necessary to find the right balance between the Zener drag force and the driving force, which determines the final recrystallized volume fraction. Considering the GNDs as an additional driving force was found to be necessary because without it, the driving force p_{driv} derived from 3IVM+ alone was too low to start any RX with the given, experimentally derived Zener drag force. An alternative approach would be to introduce a factor enhancing ρ_{i} and ρ_{w} calculated by 3IVM+. However, such an approach is unable to produce consistent results for both process routes with the same factor.

The Zener drag force in the case of route 2 (410°C) was assumed to be increased by a factor of 4. This factor is a preliminary estimation from the particle density visible in

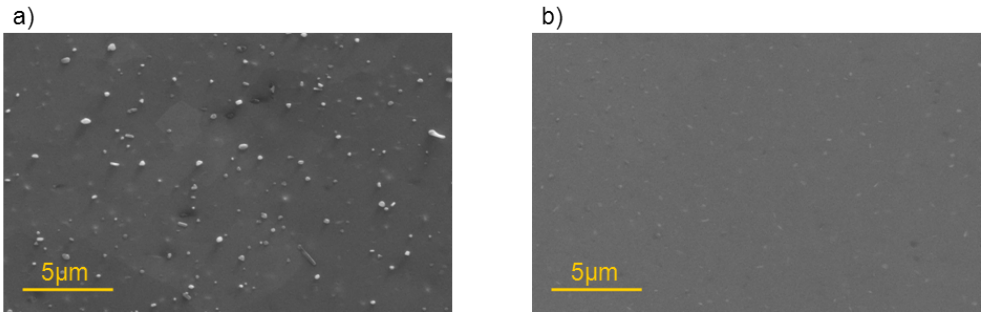

Figure 4: The state of fine particles in the material processed in a) route 2 (410°C): new precipitates formed; b) route 1 (530°C): no new precipitates were found by SEM after 2 minutes of annealing following the deformation.

figure 4.a. A quantitative characterization of these fine particles is necessary and currently in preparation, to obtain an accurate value for the corresponding Zener drag force.

6 CONCLUSIONS AND OUTLOOK

Microstructure development during hot deformation and subsequent annealing was experimentally investigated for two processing routes. Based on the experimental results, the microstructure evolution was simulated by selected models of an integrated through-process model framework.

Under several assumptions on the RX driving force as well as on the Zener drag force, the RX behavior was modeled successfully such that the predicted kinetics, the final recrystallized volume fraction, and the grain size distribution are consistent with the experiments for both processing routes. From the experimental data available, the assumptions for the existing model framework were necessary to obtain agreement with experiments. Further experimental material characterization in respect of the dislocation structure and the Zener drag are required to fully justify (or reject) the assumptions made.

7 ACKNOWLEDGEMENT

This research was carried out under the project number M42.5.09375 in the framework of the Research Program of the Materials innovation and institute M2i (www.m2i.nl). The financial support of M2i and Aleris Europe is gratefully acknowledged.

REFERENCES

[1] Crumbach, M., Pomana, G., Wagner, P. and Gottstein, G., A taylor type deformation texture model considering grain interaction and material properties. Part I fundamentals *1st Joint International Conference on Recystallization and Grain Growth.* Berlin Springer, (2001): 1053–1060.

[2] Crumbach, M., Goerdeler, M., Gottstein, G., Neumann, L., Aretz, H. and Kopp, R.,

Through-process texture modelling of aluminium alloys. *Modelling and Simulation in Materials Science and Engineering.* (2004) **12**:1–18.

[3] Roters, F., Raabe, D. and Gottstein, G., Work hardening in heterogeneous alloys a microstructural approach based on three internal state variables. *Acta Materialia.* (2000) **48**:4181–4189.

[4] Goerdeler, M. and Gottstein, G., Dislocation density based flow stress modeling. *1st Joint International Conference on Recystallization and Grain Growth.* Berlin Springer, (2001): 987–994.

[5] Goerdeler, M., Crumbach, M., Schneider, M., Gottstein, G., Neumann, L., Aretz, H. and Kopp, R., Dislocation density based modeling of work hardening in the context of integrative modeling of aluminum processing. *Materials Science and Engineering A.* (2004) **387-389**:266–271.

[6] Prasad, G., An improved dislocation density based work hardening model for Al-alloys. *PhD thesis.* RWTH Aachen University, (2007).

[7] Mohles, V., Li, X., Heering, C., Hirt, G., Bhaumik, S. and Gottstein, G., Validation of an improved dislocation density based flow stress model for Al-alloys. *11th International ESAFORM Conference on Materials Forming.* Lyon, (2008): 987–990.

[8] Crumbach, M., Through-process texture modeling. *PhD thesis.* RWTH Aachen University, (2005).

[9] Schäfer, C., Song, J. and Gottstein, G., Modeling of texture evolution in the deformation zone of second-phase particles. *Acta Materialia.* (2009) **57**:1026–1034.

[10] Derby and Ashby, M.F., On dynamic recrystallization. *Scripta Metallurgica.* (1987) **21**:879–884.

[11] Schäfer, C., Pomana, G., Mohles, V., Gottstein, G., Engler, O. and Hirsch, J., Recrystallization modeling of AA8XXX alloys with cellular automata considering recovering kinetics. *Advanced Engineering Materials.* (2010) **12**:131–140.

[12] Humphreys, F.J. and Kalu, P.N., Dislocation-particle interactions during high temperature deformation of two-phase aluminium alloys. *Acta Metallurgica.* (1987) **35**:2815–2829.

[13] Duckham, A., Knutsen, R.D. and Engler, O., Influence of deformation variables on the formation of copper-type shear bands in Al-1Mg. *Acta Materialia.* (2001) **49**:2739–2749.

[14] Schäfer, C., Recrystallization modeling considering second-phase particles. *PhD thesis.* RWTH Aachen University, (2010).